

Bayesian-based Symbol Detector for Orthogonal Time Frequency Space Modulation Systems

Xinwei Qu*, Alva Kosasih*, Wibowo Hardjawana*, Vincent Onasis*, and Branka Vucetic*

*Centre of Excellence in Telecommunications, University of Sydney, Sydney, Australia.

{alva.kosasih,wibowo.hardjawana,branka.vucetic}@sydney.edu.au,
xiqu4217@uni.sydney.edu.au, and vona0880@uni.sydney.edu.au.

Abstract—Recently, the orthogonal time frequency space (OTFS) modulation is proposed for 6G wireless system to deal with high Doppler spread. The high Doppler spread happens when the transmitted signal is reflected towards the receiver by fast moving objects (e.g. high speed cars), which causes inter-carrier interference (ICI). Recent state-of-the-art OTFS detectors fail to achieve an acceptable bit-error-rate (BER) performance as the number of mobile reflectors increases which in turn, results in high inter-carrier-interference (ICI). In this paper, we propose a novel detector for OTFS systems, referred to as the Bayesian based parallel interference and decision statistics combining (B-PIC-DSC) OTFS detector that can achieve a high BER performance, under high ICI environments. The B-PIC-DSC OTFS detector employs the PIC and DSC schemes to iteratively cancel the interference, and the Bayesian concept to take the probability measure into the consideration when refining the transmitted symbols. Our simulation results show that in contrast to the state-of-the-art OTFS detectors, the proposed detector is able to achieve a BER of less than 10^{-5} , when SNR is over 14 dB, under high ICI environments.

Index Terms—OTFS, ICI, Bayesian parallel interference cancellation, symbol detection, mobile cellular networks.

I. INTRODUCTION

The sixth-generation (6G) wireless system will support advance mobile network applications (e.g. unmanned aerial vehicles (UAV), and autonomous cars) [1], [2], which come with stringent error-rate requirement under high Doppler spread environments. For example, in the autonomous car application where there exists high mobility reflectors (i.e. the other moving vehicles around the vicinity of a specific car receiver), high Doppler spread is observed. This is shown in Fig. 1. These reflectors cause an inter-carrier interference (ICI) which significantly degrades the performance of the current orthogonal frequency division multiplexing (OFDM) systems [3]. The orthogonal time frequency space (OTFS) modulation has been proposed in [4] to tackle this issue by multiplexing the transmitted symbols in the delay-Doppler (DD) domain and then spreading them out in the time-frequency (TF) domain.

The performance of classical low complexity detectors, i.e., zero forcing (ZF) and minimum-mean-square-error (MMSE) detectors, in the OTFS system have been investigated in [5]. Despite low complexity, the classical detectors suffer a significant performance degradation, compared to the optimal maximum likelihood (ML) detector [6]. To address this issue,

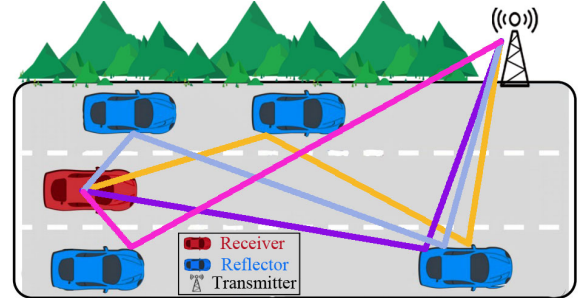


Fig. 1: High mobility reflectors

iterative receiver algorithms have been employed for the OTFS detectors based on the message passing (MP) [7], approximate message passing (AMP), and unitary transformation AMP (UTAMP) [8]. The MP based detectors, in the OTFS system, use a message passing iterative algorithm to compute the posterior probability function of the transmitted symbols, where the messages represent Gaussian approximations of the ICI. Unfortunately, the BER performance of the MP based detectors degrades due to the increase in ICI as the number of moving reflectors rises. Recently, we proposed an iterative Bayesian based detection algorithm, referred to as the Bayesian parallel interference and decision statistic combining (B-PIC-DSC). The algorithm iteratively estimates the mean and variance of the transmitted symbols and uses them to subtract interference from the received signal. The proposed algorithm is shown to achieve a significant bit-error-rate (BER) performance gain, as compared to the state-of-the-arts, in the massive multiple-input-multiple-output scenario [9].

In this paper, we propose a novel iterative OTFS detector. The detector is based on the B-PIC-DSC detection algorithm [9], referred to as the B-PIC-DSC OTFS detector. The B-PIC-DSC OTFS detector first applies the PIC scheme to remove the ICI from the received signals using the symbol estimates from the previous iteration. A factorizable Gaussian posterior belief of the transmitted symbols is then constructed based on the PIC outputs. The posterior belief of the transmitted symbols is then used to infer the soft symbol estimates. The DSC concept is then utilized to yield the final symbol estimates by weighting the soft symbol estimates in the previous and current iterations. The process is then repeated iteratively until there

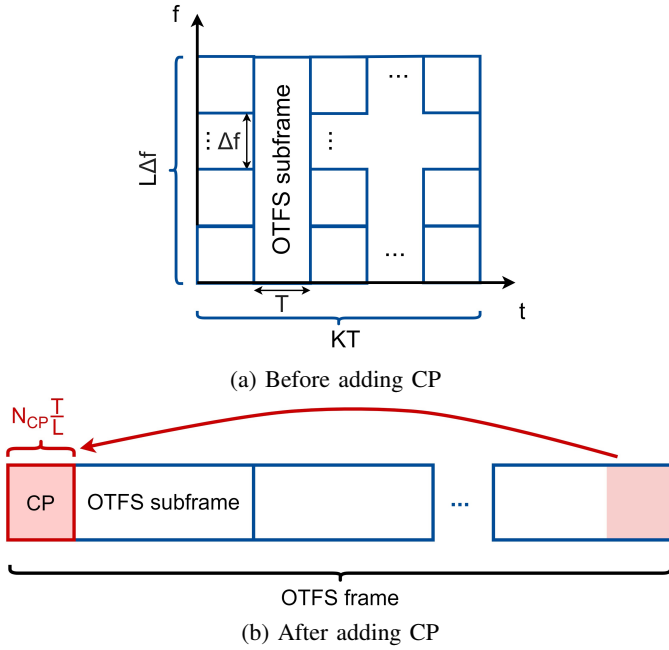


Fig. 2: An OTFS frame structure

is no significant performance improvement in the soft symbol estimates. The DSC outputs, from the last iteration, are then used to refine the transmitted symbols. The main contribution of this paper is the development of the B-PIC-DSC detector for an OTFS system that can achieve a high BER performance, in the presence of a strong ICI due to a large number of moving reflectors. The simulation results demonstrate that our proposed detector is able to achieve a BER of 10^{-5} , in the presence of a large number of high mobile reflectors. This is in contrast to other OTFS detectors that fail to work in such an environment.

Notations: a , \mathbf{a} and \mathbf{A} denote scalar, vector, and matrix respectively. $\mathbb{C}^{M \times N}$ denotes the set of $M \times N$ dimensional complex matrices. We use \mathbf{I}_N , \mathbf{F}_N , and \mathbf{F}_N^H to represent an N -dimensional identity matrix, N -points discrete Fourier Transform matrix, and N -points inverse discrete Fourier transform matrix. $(\cdot)^T$, $(\cdot)^H$, $(\cdot)^*$, and $[\cdot]_M$ represent the transpose, Hermitian, conjugate, and mod- M operations. We define $\mathbf{a} = \text{vec}(\mathbf{A})$ as the column-wise vectorization of matrix \mathbf{A} . The Kronecker product is denoted as \otimes . The Euclidean distance of vector \mathbf{x} is denoted as $\|\mathbf{x}\|$. We use $\mathcal{N}(\mathbf{x} : \boldsymbol{\mu}, \boldsymbol{\Sigma})$ to express the multivariate Gaussian distribution of a vector \mathbf{x} where $\boldsymbol{\mu}$ is the mean and $\boldsymbol{\Sigma}$ is the covariance matrix.

II. SYSTEM MODEL

We consider an OTFS system, illustrated in Fig. 3. The transmitter and receiver are equipped with a single antenna. The channel state information (CSI) is assumed to be known in the receiver side. In the following, we discuss the detail of the OTFS transmitter, channel, and receiver.

A. OTFS Transmitter

In the transmitter side, we first map the information binary sequences into the M -ary quadrature amplitude modulation (M -QAM) symbols. The constellation set of the M -QAM symbols is denoted as Ω , where the constellation size is M . The symbols, $\mathbf{X}_{\text{DD}}[l, k] \in \mathbb{C}^{L \times K}$, are assigned in the delay Doppler (DD) domain, where $l = 0, \dots, L - 1$ and $k = 0, \dots, K - 1$, are the indices of discretized delay and Doppler shifts, respectively. We transform the symbols from the DD domain into the time-frequency (TF) domain, as illustrated in Fig. 3, by using the inverse symplectic finite Fourier transform (ISFFT) [10]. Here, the TF domain is discretized to L by K grids with uniform intervals Δf (Hz) and $T = 1/\Delta f$ (seconds), respectively. Therefore, the sampling time is $\frac{T}{L}$. The TF domain samples $\mathbf{X}_{\text{TF}} \in \mathbb{C}^{L \times K}$ in an OTFS frame, which occupies the bandwidth of $L\Delta f$ and the duration of KT , is given as follows:

$$\mathbf{X}_{\text{TF}} = \mathbf{F}_L \mathbf{X}_{\text{DD}} \mathbf{F}_K^H, \quad (1)$$

where $\mathbf{F}_L \in \mathbb{C}^{L \times L}$ and $\mathbf{F}_K^H \in \mathbb{C}^{K \times K}$ are the discrete Fourier transform (DFT) and inverse DFT (IDFT) matrices¹, respectively. The (discrete) Heisenberg transform [4] is then applied to convert the TF domain samples into the time domain, referred to as the transmitted signal, i.e.,

$$\begin{aligned} \mathbf{s} &= \text{vec}(\mathbf{G}_{\text{tx}} \mathbf{F}_L^H \mathbf{X}_{\text{TF}}) \\ &= \text{vec}(\mathbf{G}_{\text{tx}} \mathbf{F}_L^H \mathbf{F}_L \mathbf{X}_{\text{DD}} \mathbf{F}_K^H) \\ &= \text{vec}(\mathbf{G}_{\text{tx}} \mathbf{X}_{\text{DD}} \mathbf{F}_K^H) \\ &= (\mathbf{F}_K^H \otimes \mathbf{G}_{\text{tx}}) \mathbf{x}_{\text{DD}}, \end{aligned} \quad (2)$$

where $\mathbf{s} \in \mathbb{C}^{KL \times 1}$ is the vector of the transmitted signal, $\mathbf{G}_{\text{tx}} = \text{diag}[g_{\text{tx}}(0), g_{\text{tx}}(T/L), \dots, g_{\text{tx}}((L-1)T/L)] \in \mathbb{C}^{L \times L}$, $\text{diag}[\cdot]$ denotes the operation to diagonalize a vector, $g_{\text{tx}}(t)$ is a rectangular waveform [11], and $\mathbf{x}_{\text{DD}} \in \mathbb{C}^{KL \times 1}$ is the vectorization of \mathbf{X}_{DD} , by using the Kronecker product rule². Note that we follow the OTFS model, considered in [12], where the cyclic prefix (CP) is only inserted in the beginning of the OTFS frame, which not only mitigates the CP overhead but also tremendously increases the spectral efficiency. Hence, for each OTFS frame, the time duration after adding CP is $KT + N_{\text{cp}} \frac{T}{L}$ and the number of samples is $KL + N_{\text{cp}}$, where N_{cp} is equal to the index of the maximum delay. The OTFS frame structure is shown in Fig. 2.

B. OTFS Wireless Channel

The OTFS wireless channel is a time-varying multipath channel, represented by the impulse responses in the delay Doppler domain, i.e.,

$$h(\tau, \nu) = \sum_{i=1}^P h_i \delta(\tau - \tau_i) \delta(\nu - \nu_i) \quad (3)$$

¹The (p, q) th entries of N -points DFT and its inverse are $(\frac{1}{\sqrt{N}} e^{-j2\pi pq/N})_{p,q=0, \dots, N-1}$ and $(\frac{1}{\sqrt{N}} e^{j2\pi pq/N})_{p,q=0, \dots, N-1}$.

²A matrix multiplication is often expressed by using vectorization with the Kronecker product. That is, $\text{vec}(ABC) = (C^T \otimes A) \text{vec}(B)$

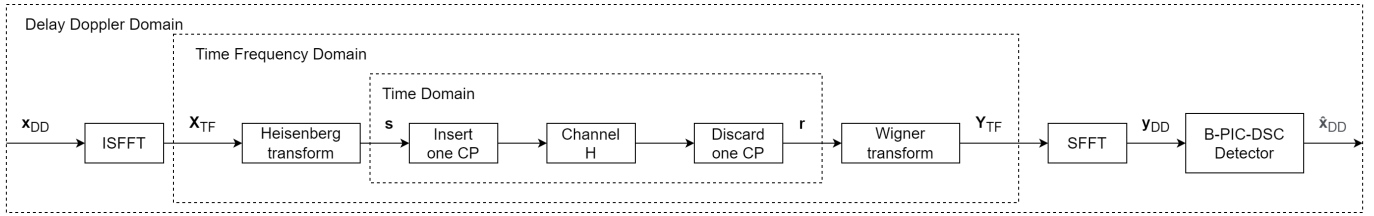


Fig. 3: The system model of OTFS modulation scheme

where $\delta(\cdot)$ is the Dirac delta function, h_i denotes the i -th path gain, and P is the total number of paths. These paths come with different delay and/or Doppler characteristics, where each of them represents the channel between moving reflectors/transmitter and the receiver. Therefore, the delay and Doppler shifts are given as

$$\tau_i = l_i \frac{T}{L}, \quad v_i = (k_i) \frac{\Delta f}{K}, \quad (4)$$

respectively. Here, the integers $l_i \in [0, l_{max}]$ and $k_i \in [-k_{max}, k_{max}]$ denote the indices of the delay and Doppler shifts, where l_{max} and k_{max} are the indices of the maximum delay and maximum Doppler shifts among all channel paths.

C. OTFS Receiver

The received signal is obtained from sending the transmitted signal \mathbf{s} over the channel $h(\tau, v)$, which includes the delay and Doppler terms. We discard the CP by removing the first N_{cp} samples from a received OTFS frame, and thus the time domain received signal is given as [13]

$$r(n) = \sum_i^P h_i e^{j2\pi \frac{k_i(n-l_i)}{KL}} s([n-l_i]_{KL}) + w(n), \quad (5)$$

where $n = 0, \dots, KL - 1$. The sampling frequency is $L\Delta f$ [12]. We can then rewrite (5) in a matrix-vector form as

$$\mathbf{r} = \mathbf{H}\mathbf{s} + \mathbf{w}, \quad (6)$$

where \mathbf{w} is the independent and identically distributed (i.i.d.) white Gaussian noise that follows $\mathcal{N}(\mathbf{0}, \sigma^2 \mathbf{I})$, σ^2 is the variance of the noise, and $\mathbf{H} = \sum_{i=1}^P h_i \mathbf{I}_{KL}(l_i) \mathbf{\Delta}(k_i)$, $\mathbf{I}_{KL}(l_i)$ denotes a $KL \times KL$ matrix obtained by circularly left shifting the columns of the identity matrix by l_i , for example when $l_i = 1$,

$$\mathbf{I}_{KL}(1) = \begin{bmatrix} 0 & \cdots & 0 & 1 \\ 1 & \ddots & 0 & 0 \\ \vdots & \ddots & \ddots & \vdots \\ 0 & \cdots & 1 & 0 \end{bmatrix}.$$

Furthermore, $\mathbf{\Delta}$ is the $KL \times KL$ diagonal matrix from the Doppler shifts, i.e.,

$$\mathbf{\Delta}(k_i) = \text{diag} \left[e^{\frac{j2\pi k_i(0)}{KL}}, e^{\frac{j2\pi k_i(1)}{KL}}, \dots, e^{\frac{j2\pi k_i(KL-1)}{KL}} \right].$$

Note that the matrices $\mathbf{I}_{KL}(l_i)$ and $\mathbf{\Delta}(k_i)$ describe the delay and Doppler shifts in (5), respectively. We define a matrix

$$\mathbf{R} \triangleq \begin{bmatrix} r(0) & r(L) & \cdots & r((K-1)L) \\ r(1) & r(L+1) & \cdots & r((K-1)L+1) \\ \vdots & \vdots & \cdots & \vdots \\ r(L-1) & r(2L-1) & \cdots & r(KL-1) \end{bmatrix}.$$

As shown in Fig. 3, we convert the received signal into the TF domain by applying the Wigner transform [12], which yields

$$\mathbf{Y}_{TF} = \mathbf{F}_L \mathbf{G}_{rx} \mathbf{R}, \quad (7)$$

where $\mathbf{G}_{rx} = \text{diag} [g_{rx}(0), g_{rx}(T/L), \dots, g_{rx}((L-1)T/L)] \in \mathbb{C}^{L \times L}$ and $g_{rx}(t)$ is the rectangular waveform in the receiver. We then use the symplectic finite Fourier transform (SFFT) [10] to obtain the received signal in the DD domain, i.e.,

$$\begin{aligned} \mathbf{Y}_{DD} &= \mathbf{F}_L^H \mathbf{Y}_{TF} \mathbf{F}_K \\ &= \mathbf{F}_L^H \mathbf{F}_L \mathbf{G}_{rx} \mathbf{R} \mathbf{F}_K \\ &= \mathbf{G}_{rx} \mathbf{R} \mathbf{F}_K. \end{aligned} \quad (8)$$

By following the vectorization with Kronecker product rule, we can rewrite (8) as

$$\begin{aligned} \mathbf{y}_{DD} &= \text{vec}(\mathbf{Y}_{DD}) \\ &= \text{vec}(\mathbf{G}_{rx} \mathbf{R} \mathbf{F}_K) \\ &= (\mathbf{F}_K \otimes \mathbf{G}_{rx}) \mathbf{r}. \end{aligned} \quad (9)$$

By first substituting \mathbf{s} in (2) into (6) and using the result to replace \mathbf{r} in (9), we obtain

$$\mathbf{y}_{DD} = \mathbf{H}_{\text{eff}} \mathbf{x}_{DD} + \tilde{\mathbf{w}}, \quad (10)$$

where $\mathbf{H}_{\text{eff}} = (\mathbf{F}_K \otimes \mathbf{G}_{rx}) \mathbf{H} (\mathbf{F}_K^H \otimes \mathbf{G}_{tx})$ and $\tilde{\mathbf{w}} = (\mathbf{F}_K \otimes \mathbf{G}_{rx}) \mathbf{w}$ denote the effective channel and noise in the DD domain, respectively. Here, $\tilde{\mathbf{w}}$ is an i.i.d. Gaussian noise, since $\mathbf{F}_K \otimes \mathbf{G}_{rx}$ is a unitary orthogonal matrix [4], [12].

III. B-PIC-DSC OTFS DETECTOR

In this section, we describe the development of the B-PIC-DSC detector [9] for an OTFS system. The structure of the B-PIC-DSC detector is illustrated in Fig. 4. It consists of three modules: Bayesian symbol observation (BSO), Bayesian symbol estimation (BSE), and DSC modules. Note that in the following discussion we consider the DD domain received signal, where the expression is given in (10). In the following, we omit the subscripts DD and eff for notational simplicity.

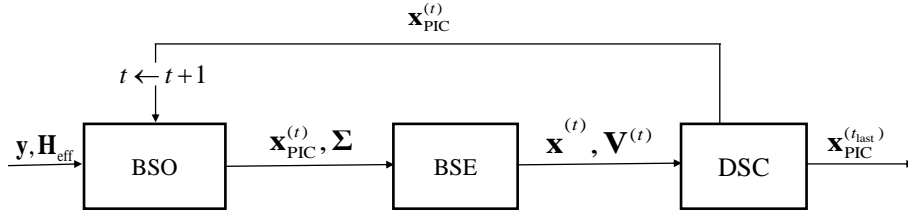


Fig. 4: B-PIC-DSC Detector

A. Bayesian Symbol Observation

In the BSO module, the transmitted symbols \mathbf{x} in (10) is treated as a random vector. The posterior function of $\mathbf{x} = [x_1, \dots, x_q, \dots, x_{KL}]$, given the received signals $\mathbf{y} = [y_1, \dots, y_c, \dots, y_{KL}]$, is expressed as

$$p(\mathbf{x}|\mathbf{y}) = \frac{p(\mathbf{y}|\mathbf{x})p(\mathbf{x})}{p(\mathbf{y})}, \quad (11)$$

where $p(\mathbf{y}|\mathbf{x}) = \mathcal{N}(\mathbf{y}, \mathbf{H}\mathbf{x}; \sigma^2\mathbf{I})$. Following [9], we iteratively approximate the posterior probability $p(\mathbf{x}|\mathbf{y})$ by a product of independent Gaussian functions expressed as

$$p(\mathbf{x}|\mathbf{y}) \approx \prod_{q=1}^{KL} \underbrace{\mathcal{N}(x_q, x_{\text{PIC},q}^{(t)}; \Sigma_q^{(t)})}_{\hat{p}^{(t)}(x_q|\mathbf{y})}. \quad (12)$$

Here, $x_{\text{PIC},q}^{(t)}$ is the soft estimate of x_q in iteration t , obtained from the matched filter based PIC scheme, given as follows:

$$x_{\text{PIC},q}^{(t)} = \frac{\mathbf{h}_q^H (\mathbf{y} - \mathbf{H}\mathbf{x}_{\text{PIC}\setminus q}^{(t-1)})}{\|\mathbf{h}_q\|^2}, \quad (13)$$

where \mathbf{h}_q is the q -th column of matrix \mathbf{H} and

$$\mathbf{x}_{\text{PIC}\setminus q}^{(t-1)} = [x_{\text{PIC},1}^{(t-1)}, \dots, x_{\text{PIC},q-1}^{(t-1)}, 0, x_{\text{PIC},q+1}^{(t-1)}, \dots, x_{\text{PIC},KL}^{(t-1)}]^T$$

is the estimated symbols in the $(t-1)$ -th iteration. Note that we use the MMSE scheme to produce the initial value of the q -th symbol estimate, that is,

$$x_{\text{PIC},q}^{(0)} = (\mathbf{h}_q^H \mathbf{h}_q + \sigma^2)^{-1} \mathbf{h}_q^H \mathbf{y}. \quad (14)$$

Remark 1: The MMSE initialization given in (14) is necessary to improve the performance of the maximum ratio combining (MRC) based B-PIC-DSC detector proposed in [9], especially in the presence of high interference. Such high interference is encountered in the OTFS systems when there is a large number of moving reflectors, namely, high ICI. The variance Σ_q of the q -th PIC symbol estimate is approximated in [9] as

$$\Sigma_q = \frac{\sigma^2}{\sum_{c=1}^{KL} h_{c,q}^* h_{c,q}}. \quad (15)$$

The approximated posterior functions, $\hat{p}^{(t)}(x_q|\mathbf{y}) = \mathcal{N}(x_q, x_{\text{PIC},q}^{(t)}; \Sigma_q^{(t)})$, $q = 1, \dots, KL$, are then forwarded to the BSE module, as shown in Fig. 4.

B. Bayesian Symbol Estimator

In the BSE module, we compute the Bayesian symbol estimate of the q -th symbol by using $\hat{p}^{(t)}(x_q|\mathbf{y})$ obtained from the BSO module. Based on the factorization of $p(\mathbf{x}|\mathbf{y})$ in (12), we infer the symbol estimate $\hat{x}_q^{(t)}$ by using the maximum a posteriori criterion, given as

$$\hat{x}_q^{(t)} = \arg \max_{a \in \Omega} \hat{p}^{(t)}(x_q = a|\mathbf{y}). \quad (16)$$

Note that the MAP criterion in (16) has a linear complexity since the inference is performed for each q -th symbol estimate. The Bayesian symbol estimate and its variance are respectively given as

$$\hat{x}_q^{(t)} = \mathbb{E} [x_q | x_{\text{PIC},q}^{(t)}, \Sigma_q] = \sum_{a \in \Omega} a \hat{p}^{(t)}(x_q = a|\mathbf{y}) \quad (17)$$

$$V_q^{(t)} = \mathbb{E} \left[\left| x_q - \mathbb{E} [x_q | x_{\text{PIC},q}^{(t)}, \Sigma_q] \right|^2 \right], \quad (18)$$

where $\hat{p}^{(t)}(x_q|\mathbf{y})$ is normalized so that $\sum_{a \in \Omega} \hat{p}^{(t)}(x_q = a|\mathbf{y}) = 1$. The outputs of the BSE module, $\hat{x}_q^{(t)}$ and $V_q^{(t)}$, $q = 1, \dots, K$, are then sent to the DSC module.

C. Decision Statistics Combining

The correlation between $\hat{x}_q^{(t)}$ and $\hat{x}_q^{(t-1)}$ in the B-PIC-DSC detector is low in the early iteration stages [9]. Such a feature can be exploited to increase the diversity of symbol estimates by forming decision statistics, referred to as the DSC concept [14]. The decision statistics consist of a linear combination of the symbol estimates in two consecutive iterations

$$x_{\text{DSC},q}^{(t)} = (1 - \rho_{\text{DSC},q}^{(t)}) \hat{x}_q^{(t-1)} + \rho_{\text{DSC},q}^{(t)} \hat{x}_q^{(t)} \quad (19)$$

The weighting coefficient,

$$\rho_{\text{DSC},q}^{(t)} = \frac{e_q^{(t-1)}}{e_q^{(t)} + e_q^{(t-1)}}, \quad (20)$$

is determined by maximizing the signal-to-interference-plus-noise-ratio (SINR). Here, $e_q^{(t)}$ is defined as the instantaneous square error of the q -th symbol estimate, computed by using the MRC filter,

$$e_q^{(t)} = \left\| \frac{\mathbf{h}_q^H}{\|\mathbf{h}_q\|^2} (\mathbf{y} - \mathbf{H}\hat{\mathbf{x}}^{(t)}) \right\|^2. \quad (21)$$

Detector	Complexity
MMSE OTFS	$\mathcal{O}(K^3L^3)$
MP OTFS	$\mathcal{O}(KLPMt_{\text{last}})$
AMP OTFS	$\mathcal{O}(K^2L^2t_{\text{last}})$
UTAMP OTFS	$\mathcal{O}(L^2K + LKM)$
B-PIC-DSC OTFS	$\mathcal{O}(K^3L^3 + K^2L^2t_{\text{last}})$

Table I: Computational complexity comparison

The iterative process is terminated if the following condition is satisfied,

$$\|x_{\text{DSC},q}^{(t)} - x_{\text{DSC},q}^{(t-1)}\| \leq \zeta \text{ or } t = t_{\text{max}}, \quad (22)$$

where ζ is the minimum acceptable difference of $x_{\text{DSC},q}^{(t)}$ in two consecutive iterations, and t_{max} is the maximum number of iterations. We then use $x_{\text{DSC},q}^{(t)}$ as the input of the BSO module by assigning the value of $x_{\text{DSC},q}^{(t)}$ to $x_{\text{PIC},q}^{(t)}$,

$$x_{\text{PIC},q}^{(t)} \leftarrow x_{\text{DSC},q}^{(t)}, \quad (23)$$

Algorithm 1 The B-PIC-DSC OTFS detector

```

1: Input:  $K, \Omega, \mathbf{y}, \mathbf{H}, \sigma^2, V_q^{(0)} \leftarrow 1, t_{\text{max}} \leftarrow 10$ 
2: Output:  $\hat{\mathbf{x}}^{(T)}$ 
3: for  $t = 1, \dots, t_{\text{max}}$  do
4:   for  $q = 1, \dots, KL$  (or parallel execution) do
5:     The BSO Module:
6:     if  $t = 0$  then
7:       Compute (14)
8:     end if
9:     Compute  $x_{\text{PIC},q}^{(t)}$  in (13)
10:    Compute the variance  $\Sigma_q$  in (15)
11:    The BSE Module:
12:    Compute the Bayesian symbol estimate  $\hat{x}_q^{(t)}$  in (17)
13:    Compute the Bayesian variance  $V_q^{(t)}$  in (18)
14:    The DSC Module:
15:    Compute  $e_q^{(t)}$  in (21)
16:    Compute  $\rho_{\text{DSC},q}^{(t)}$  in (20)
17:    Compute  $x_{\text{DSC},q}^{(t)}$  in (19)
18:    Compute (23)
19:   end for
20:   if  $\|x_{\text{DSC},q}^{(t)} - x_{\text{DSC},q}^{(t-1)}\| \leq 10^{-4}$  then
21:     break
22:   end if
23: end for
24:  $t_{\text{last}} \leftarrow t$ 

```

The complete pseudo-code of the B-PIC-DSC OTFS detector is shown in Algorithm 1.

IV. COMPLEXITY ANALYSIS

In this section, we analyze the complexity of the proposed B-PIC-DSC OTFS detector. Algorithm 1 specifies that the B-PIC-DSC OTFS detector performs matrix vector multiplications in (13), (15)-(21), at each iteration and therefore the cost

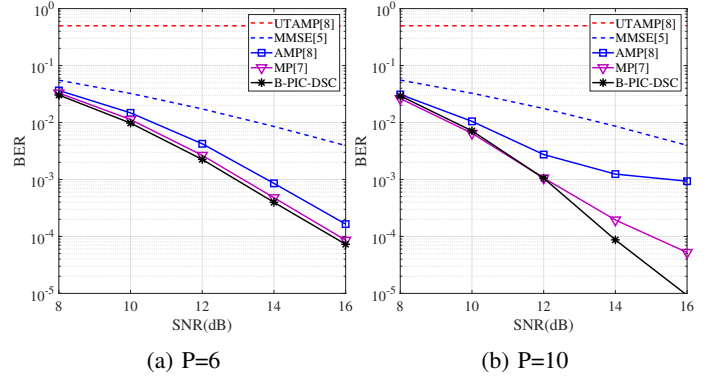


Fig. 5: A moderate number of mobile reflectors with $k_{\text{max}} = 1$

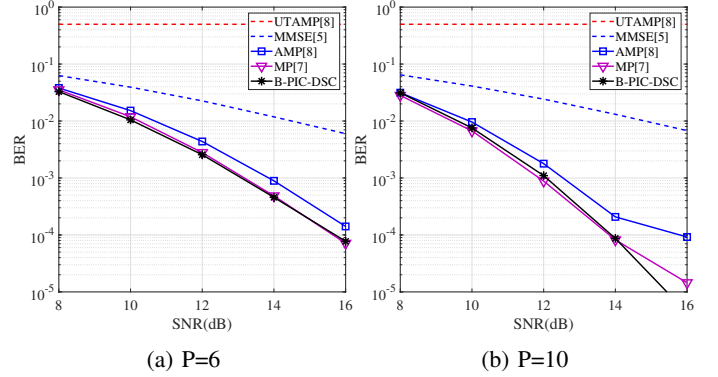


Fig. 6: A moderate number of mobile reflectors with $k_{\text{max}} = 3$

is $\mathcal{O}(K^2L^2t_{\text{last}})$, where t_{last} denotes the number of iterations. The matrix inverse operation, performed in the first iteration, given in (14), requires $\mathcal{O}(K^3L^3)$ computational complexity. Hence the overall complexity of the B-PIC-DSC OTFS detector is $\mathcal{O}(K^3L^3 + K^2L^2t_{\text{last}})$. This complexity is similar to that of the MMSE OTFS detector. The computational complexity of the MP OTFS, AMP OTFS, and UTAMP OTFS detectors are tabulated in Table 1. Although the proposed B-PIC-DSC OTFS detector has a higher complexity compared to the other detectors, this comes with a significant BER performance gain in the presence of strong ICI, resulted from the presence of a large number of reflectors, as will be discussed in the next section.

V. NUMERICAL RESULTS

In this section, we evaluate the performance of our detector by comparing the BER of our proposed detector with that of the MMSE OTFS [7], MP OTFS [15], AMP OTFS [16], and UTAMP OTFS [8] detectors. We set $L = 12$, $K = 7$, and $\Delta f = 15\text{kHz}$. In the channel, the delay index is $l_i \in [1, 6]$ excluding the first path ($l_i = 0$), the Doppler shift index of i -th path, k_i , is uniformly drawn from $[-1, 1]$ or $[-3, 3]$ and the path gain h_i is independently drawn from the complex Gaussian distribution $\mathcal{N}(0, 1/P)$. The 4-QAM modulation is employed for the simulations. The number of of the trans-

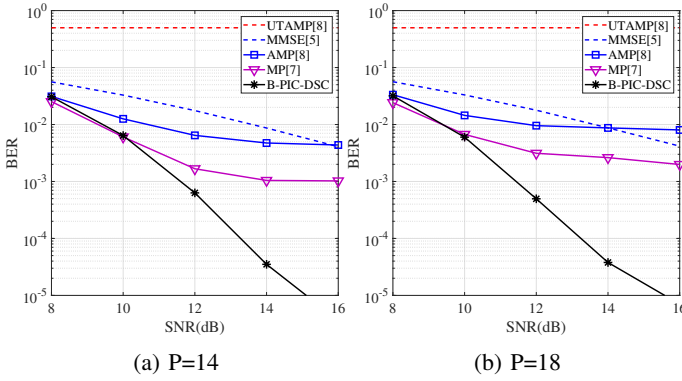


Fig. 7: A large number of mobile reflectors with $k_{max} = 1$

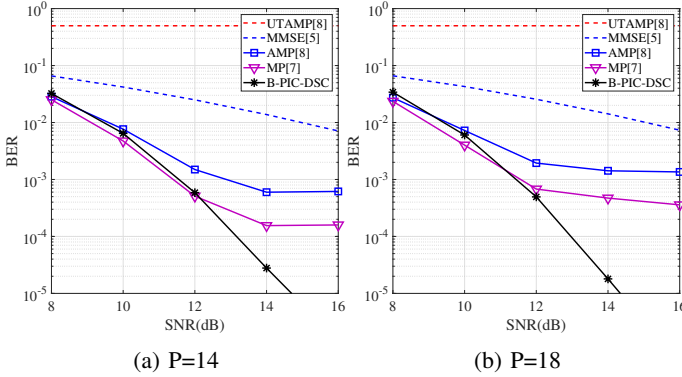


Fig. 8: A large number of mobile reflectors with $k_{max} = 3$

mitted QAM symbols per OTFS frame is $KL = 84$ and the number of samples in CP is $N_{CP} = 6$.

We first consider two numbers of paths $P = 6$ and $P = 10$. The simulation results are shown in the Figs. 5 and 6. Here, the UTAMP OTFS detector fails to achieve an acceptable detection performance. This is because the unitary transformation is not applicable in our system model. Additionally, the MP OTFS detector outperforms the AMP and MMSE detectors. Nevertheless, the B-PIC-DSC OTFS detector can achieve the lowest BER in comparison to the other counterparts.

We then increase the numbers of paths $P = 14$ and $P = 18$ as illustrated in Figs. 7 and 8. The MP based detectors can only achieve a BER performance of 10^{-4} at best, indicating that these detectors cannot handle a high ICI issue, in the OTFS system. In contrast to those existing OTFS detectors, the BER of the B-PIC-DSC OTFS detector reaches a BER less than 10^{-5} , when SNR is over 14 dB. Therefore, we conclude that our proposed detector significantly outperforms the state-of-the-art OTFS detectors.

VI. CONCLUSION

We propose the B-PIC-DSC detector for the OTFS systems that is able to achieve a high detection performance, particularly under high ICI environment, where there is a large number of moving reflectors. Our simulation results show that the B-PIC-DSC OTFS detector outperforms the state-

of-the-arts OTFS detectors with slightly higher computational complexity.

ACKNOWLEDGMENT

This research was supported by the research training program stipend from The University of Sydney. The work of Branka Vucetic was supported in part by the Australian Research Council Laureate Fellowship grant number FL160100032.

REFERENCES

- [1] N. Hashimoto, N. Osawa, K. Yamazaki, and S. Ibi. Channel estimation and equalization for CP-OFDM-based OTFS in fractional doppler channels. [Online]. Available: <https://arxiv.org/abs/2010.15396>
- [2] C.-X. Wang, J. Huang, H. Wang, X. Gao, X. You, and Y. Hao, "6G wireless channel measurements and models: Trends and challenges," *IEEE Veh. Technol. Mag.*, vol. 15, no. 4, pp. 22–32, December 2020.
- [3] T. Jiang, H.-H. Chen, H.-C. Wu, and Y. Yi, "Channel modeling and inter-carrier interference analysis for V2V communication systems in frequency-dispersive channels," *Mob. Netw. Appl.*, vol. 15, no. 1, pp. 4–12, May 2010.
- [4] R. Hadani, S. Rakib, M. Tsatsanis, A. Monk, A. J. Goldsmith, A. F. Molisch, and R. Calderbank, "Orthogonal time frequency space modulation," in *Proc. IEEE Wireless Communications and Networking Conference (WCNC)*, San Francisco, CA, USA, March 2017.
- [5] P. Singh, A. Gupta, H. B. Mishra, and R. Budhiraja. Low-complexity ZF/MMSE receivers for MIMO-OTFS systems with imperfect CSI. [Online]. Available: <https://arxiv.org/abs/2010.04057>
- [6] K. Murali and A. Chockalingam, "On OTFS modulation for high-Doppler fading channels," in *Proc. IEEE Information Theory and Applications Workshop (ITA)*, San Diego, CA, USA, February 2018.
- [7] P. Raviteja, K. T. Phan, Y. Hong, and E. Viterbo, "Interference cancellation and iterative detection for orthogonal time frequency space modulation," *IEEE Trans. Wirel. Commun.*, vol. 17, no. 10, pp. 6501–6515, August 2018.
- [8] Z. Yuan, F. Liu, W. Yuan, Q. Guo, Z. Wang, and J. Yuan. Iterative detection for orthogonal time frequency space modulation using approximate message passing with unitary transformation. [Online]. Available: <https://arxiv.org/abs/2008.06688>
- [9] A. Kosasih, W. Hardjawana, B. Vucetic, and C. K. Wen, "A linear bayesian learning receiver scheme for massive MIMO systems," in *2020 IEEE Wireless Communications and Networking Conference (WCNC)*, Gwanak-gu, Seoul, South Korea, May 2020.
- [10] A. J. Janssen, "The zak transform: A signal transform for sampled time-continuous signals," *Philips J. Res.*, vol. 43, no. 1, pp. 23–69, January 1988.
- [11] W. Mecklenbrauker, *A tutorial on non-parametric bilinear time-frequency signal representations*. Time and Frequency Representation of Signals and Systems (Eds. G Longo and B. Picinbono), 1989, vol. 309.
- [12] P. Raviteja, Y. Hong, E. Viterbo, and E. Biglieri, "Practical pulse-shaping waveforms for reduced-cyclic-prefix OTFS," *IEEE Trans. Veh. Technol.*, vol. 68, no. 1, pp. 957–961, October 2018.
- [13] M. Guillaud and D. T. Slock, "Channel modeling and associated inter-carrier interference equalization for ofdm systems with high doppler spread," in *2003 IEEE International Conference on Acoustics, Speech, and Signal Processing (ICASSP)*, Hong Kong, China, April 2003.
- [14] B. Vucetic and J. Yuan, *Space-time coding*. New York: John Wiley & Sons, 2003.
- [15] G. Caire, R. R. Muller, and T. Tanaka, "Iterative multiuser joint decoding: Optimal power allocation and low-complexity implementation," *IEEE Trans. Inf. Theory*, vol. 50, no. 9, pp. 1950–1973, August 2004.
- [16] M. Khumalo, W.-T. Shi, and C.-K. Wen, "Fixed-point implementation of approximate message passing (AMP) algorithm in massive MIMO systems," *Digit. Commun. Netw.*, vol. 2, no. 4, pp. 218–224, September 2016.